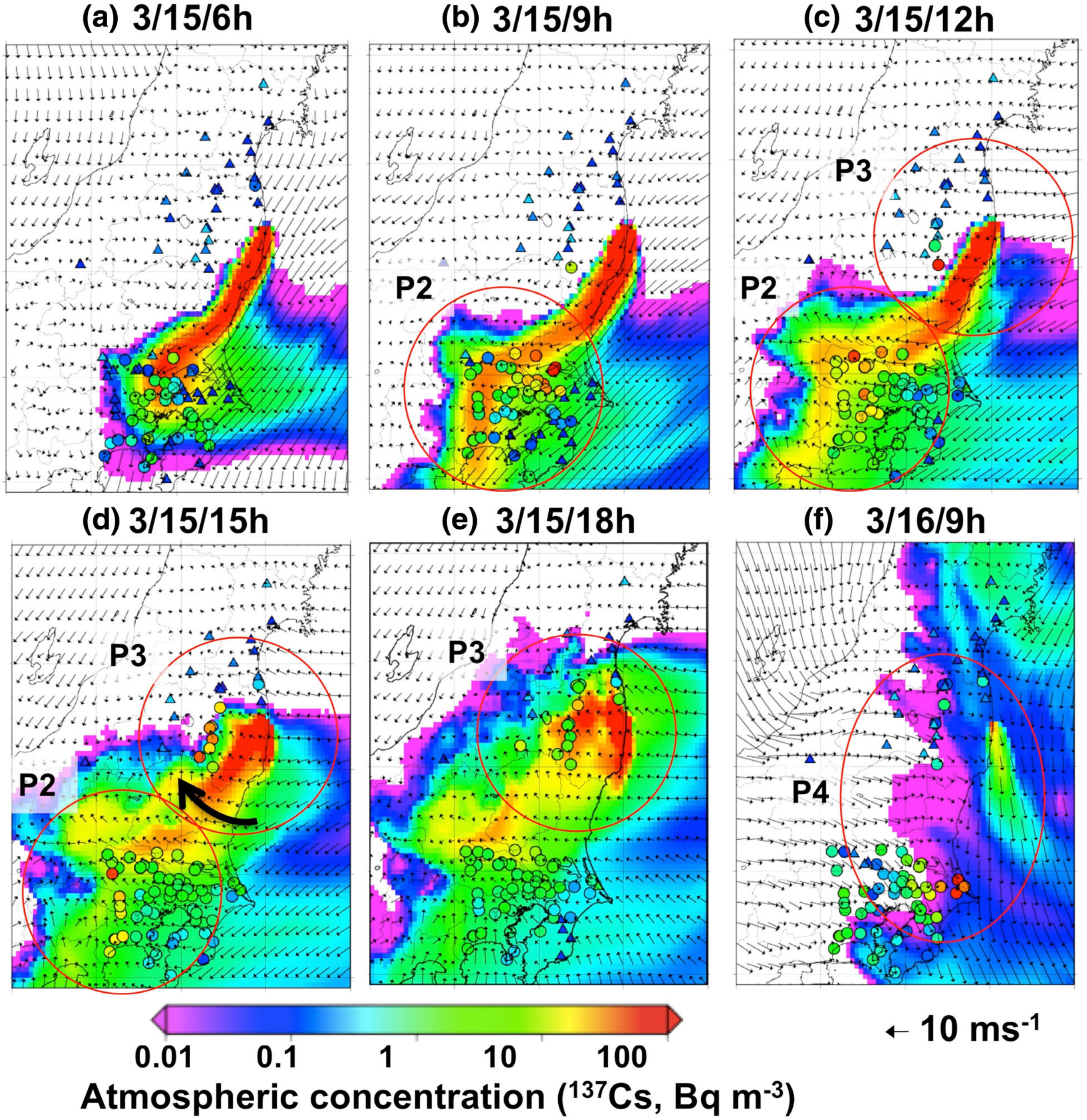

Fig. 9 a–**f** Maps of observations (*colored circles*) and model ensemble means of atmospheric ^{137}Cs concentration from 3/15/9 h to 3/16/9 h. Areas identified as plumes with concentration larger than 10 Bq m^{-3} are *encircled* and labeled with the name of the plume. JMA-MANAL wind vectors at 1000 hPa are superimposed. Movement of the P3 plume route is indicated by a *thick arrow* in panel **d**

material, due to a patch of precipitation between FDNSP and Kantou; however, the W-model simulation showed a slower dissipation.

The wind vector fields shown in Fig. 9c, d indicate that a weak cyclonic motion around the Central Fukushima area was generated until noon of 15 March; this was probably due to solar heating. It cause a gradual spread of plume P2 toward the western part of the Tokyo area, as indicated by a thick arrow in Fig. 9d. The wind field also transported plume P3 toward the Nakadori region in the afternoon of 15 March, when high concentrations of more than 100 Bq m^{-3} were observed consecutively from southern to northern sites (Fig. 6, panels 12:00 to 15:00, and Fig. 9c, d). In the late afternoon, a southeasterly wind became dominant at the FDNSP, and consequently, a part of the P3 plume took a northern detour to the edge of the Abukuma mountains and into the Nakadori region from north to south, as shown by

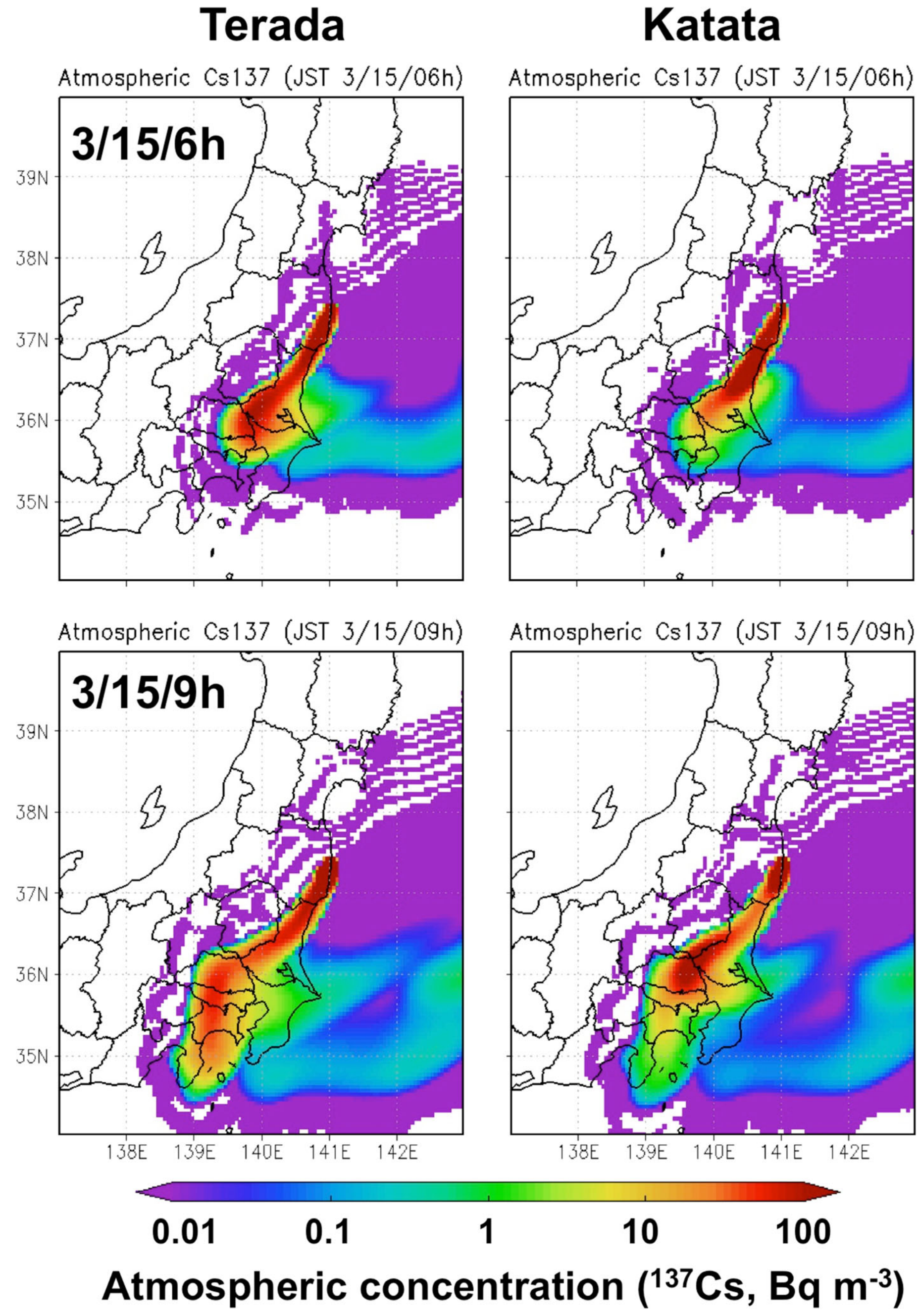

Fig. 10 Atmospheric ^{137}Cs distributions simulated by the N-model at 3/15/6 h and 3/15/9 h with emission scenarios by Terada et al. (2012) and Katata et al. (2015)

Fig. 6b, panels 15:00 to 18:00, and Fig. 9e. Tsuruta et al. (2014) also identified this northern branch. However, Figs. 6b and 9e show that without the plumes crossing the Abukuma mountains, the simulated plumes were too narrow to explain the elevated observed concentrations at the SPM sites in the Nakadori region. This problem is probably due to the spatial resolution (3–5 km), which is too coarse to simulate the fine-scale orographic horizontal advection of the plume traversing the Abukuma Mountains.

Subsequently, precipitation occurred over the Nakadori and Hamadori regions during the night of 15 March, lasting until the morning of 16 March and dissipating plume P3, as shown in Fig. 6b, panels 7:00 to 9:00, and Fig. 9f. These figures indicate that the next plume, P4, was transported by a northerly wind that became dominant during the morning of March 16, due to increased activity of the low in the Pacific (Fig. 4b). The SPM sites in the Choshi Peninsula observed a high concentration for several hours during the morning of 16 March, although the simulated plume failed to reach the target area (Fig. 9f). A possible explanation for the model failure is that the simulated aerosol height was higher than the actual height. According to the JMA analysis, there was considerable wind shear during the morning of 16 March, i.e., a northeasterly wind prevailed below 600 m, and a northwesterly wind prevailed above 600 m, as indicated by the vertical profiles of the atmosphere at the JMA Tsukuba station (36.06° N, 140.13° E) shown in Fig. 11. In a trajectory analysis using MANAL data, Miyasaka (Takafumi Miyasaka, University of Tokyo, personal communication, 2015) estimated that the aerosol height for the air mass that reached the Kantou region should be lower than 500 m. However, at the latitude 36.7° N, the simulated aerosols were distributed up to an altitude of 1500 m. Consequently, the simulated aerosols were transported to the Pacific area once they were uplifted to that level; this is indicated by the fact that the plume is not parallel to the 1000-hPa wind vector. There is a report that NICAM-SPRINTARS tends to overestimate the vertical transport of aerosols (Goto et al. 2015b). Another possible reason is overestimation of the wet deposition by the early morning precipitation along the plume on 16 March; the simulation showed this to be shifted slightly southward and was more than the MANAL objective analysis, as indicated by Fig. 6b, panel 3:00.

Another notable difference between observations and the model is that in plume P2, a medium-level concentration of between 1 and 10 Bq m^{-3} was persistently observed in a wide area of Kantou from the evening of 15 March until the morning of 16 March (Fig. 6b, panels 3/16/0:00 to 7:00; Fig. 9f), whereas the simulation results, in particular, those of the W-model, show a much smaller concentration in the southern part of the Hamadori and Kantou regions. Thus far, it is difficult for us to identify the cause of the model failures for plumes 2 and 4, but it is natural to assume that this is due to the difficulty of accurately simulating transport in a strongly sheared, thin atmosphere.

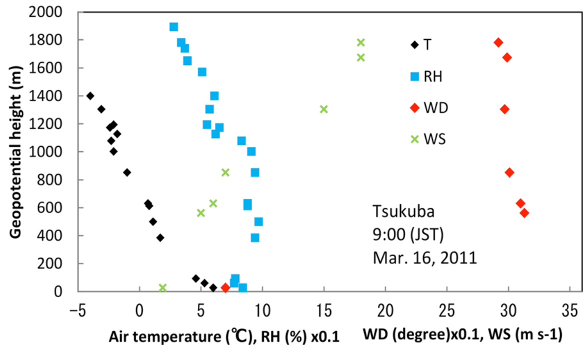

Fig. 11 Vertical profiles of temperature (*T*), relative humidity (*RH*), wind direction (*WD*), and wind speed (*WS*) versus geopotential height at 3/16/9 h for the JMA Tsukuba station. Wind directions and speeds are at the heights corresponding to the standard isobaric surfaces and characteristic points in the wind profile as determined by the JMA routine measurement protocol

18–19 March

Figure 12a, b shows the observed and simulated plumes P5 and P6 in the short-period events of 18 and 19 March. A migrating high-pressure system passed the Japanese islands on those days (Fig. 4c, d), and a weak wind condition was established around the FDNPS. The northwesterly component of the wind field turned southwesterly along the outskirts of the high-pressure zone at approximately 15:00 on 18 March (not shown). The P5 plume driven by the southwesterly wind was subsequently observed at sites north of the FDNPS. It should be noted that the wind vector at 18:00 was relatively perpendicular to the plume with this transport mechanism. A similar oblique relation between the wind vector and the plume axis was also simulated for plume P3 (Fig. 9d) and plumes P7 and P9 (shown below in Fig. 13b, f) under quick changes in the dominant wind direction. These phenomena indicate that the temporal change in wind direction must be accurately reproduced in order to successfully simulate the plume. Moreover, it is also necessary to have higher resolution of the land-sea breeze simulation.

20–21 March

A subsequent low-pressure system passed the Japanese islands during 20–21 March (Fig. 4e, f). Time sequences of observed and two-model atmospheric ^{137}Cs concentrations with precipitation maps are shown in Fig. 7, and model ensemble results are shown in Fig. 13 for several characteristic times. The figures indicate the dominant westerly wind on 19 March through the early morning of 20 March at the FDNPS blew the plume toward the Pacific, as shown in Fig. 13a (labeled A) and Fig. 7a, panel 6:00; however, during the morning of 20 March, there was an increasing easterly component due to a moving low-pressure system; this blew the plume back westward toward the Hamadori and established plume P7 (labeled B in Fig. 13a), which had a wide distribution covering the Hamadori and its offshore areas, as shown in Fig. 7a, panels 9:00 to 12:00, and Fig. 13a, b. This plume movement is indicated by a thick arrow in Fig. 13a. The simulated distribution of plume P7, however, was very different in the N- and W-models, resulting in a two-branch pattern of the ensemble mean (A and B in Fig. 13a).

The arrival of P7 at the Choshi Peninsula between 12:00 and 13:00, and its gradual westward spread until 15:00, as shown by the rotation of the plume indicated

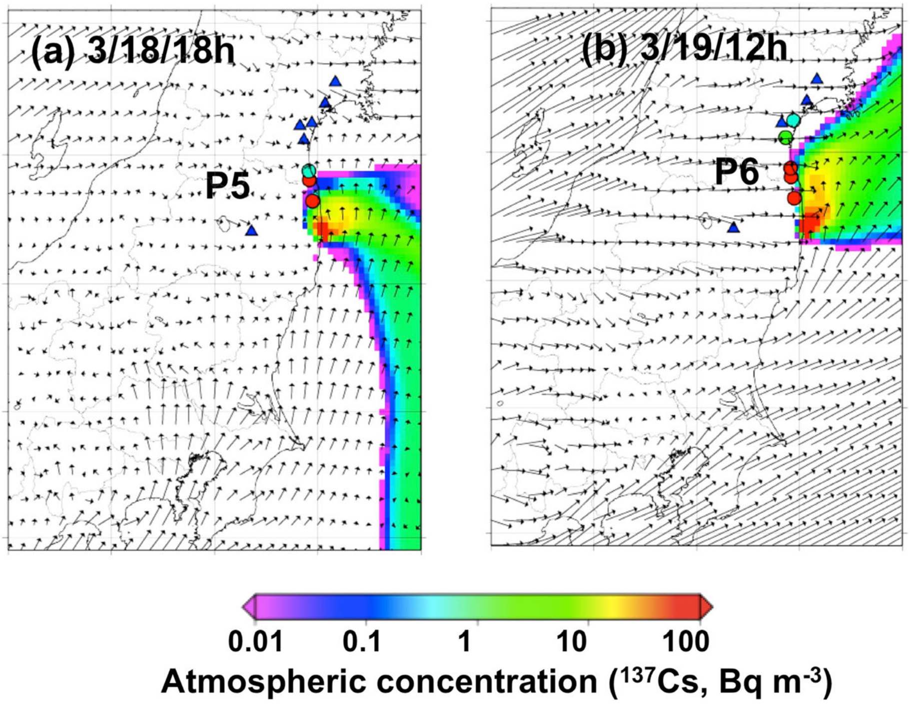

Fig. 12 Maps of observations (*colored circles*) and model ensemble means of atmospheric ^{137}Cs concentration in **a** 3/18/18 h and **b** 3/19/12 h. Areas identified as plumes with concentration larger than 10 Bq m^{-3} are *encircled* and labeled with the name of the plume. JMA-MANAL wind vectors at 1000 hPa are superimposed

by a thick arrow in Fig. 13a, was successfully simulated by the N-model, as shown in Fig. 7a, panels 12:00 to 15:00. On the other hand, the W-model failed to simulate this phenomenon. Since precipitation was not involved in the transport process on the morning of 20 March, this failure was considered to be a consequence of more transportation to the upper atmosphere near the emission source, as suggested by the shift to the north (relative to the results of the N-model) of the high concentration around the FDNPS (Fig. 7a, panels 12:00 to 13:00).

Northwestern transport started around 13:00 and lasted until that night, forming plume P8 in the Tohoku region (Fig. 7a, panels 15:00 to 21:00, and Fig. 13b, c). Each model satisfactorily simulates the transportation of plume P8 to the northern part of the Nakadori region, but they are both too coarse to simulate the successive increase in the concentration of ^{137}Cs observed from north to south along the Nakadori channel.

Plumes P7 and P8 started to dissipate at around 3:00 on March 21 (Fig. 7b, panels 1:00 to 7:00, and Fig. 13e). At this time, plume P9 started traveling to Kantou, due to a northeasterly wind ascribed to the combined effect of a migratory system and the Okhotsk low-pressure system (Fig. 4f). Plume P9 reached the Kantou region at around 9:00 on 21 March and collided with the weather front located at the southern part of the Kantou region, as shown by the wind vectors in Fig. 13f. The plume simulated by the N-model had a tongue shape and covered the land area of the northern Chiba prefecture; this was consistent with the distribution of the observed sites characterized by concentrations of more than 100 Bq m^{-3} around the Chiba prefecture and Tokyo Bay, as depicted in Fig. 7b, panels 9:00 to 10:00. However, the N-model plume was too short, and it shifted to the northern area without reaching the observed sites. In this event, the W-model also failed to transport ^{137}Cs to the Kantou region. Although not shown by a figure, we found that changing the emission scenario to that of Katata et al. (2015) did not improve the results. Another possibility is that the height of the aerosol layer was overestimated. Figure 14 shows the vertical profile of meteorological parameters at the JMA Tsukuba station at 9:00 on 21 March. The figure indicates that there was a strong temperature inversion at around 300 m geopotential height. Wind was northeasterly below the inversion and northwesterly above. Therefore, it can be assumed that the modeled aerosol layer was too high, and the aerosols were transported eastward by the northwesterly. This also might be due to the stronger precipitation that was simulated by the models in the Kantou region during the time period 3:00 to 7:00 (Fig. 13b, panels 3:00 to 7:00). These two reasons may

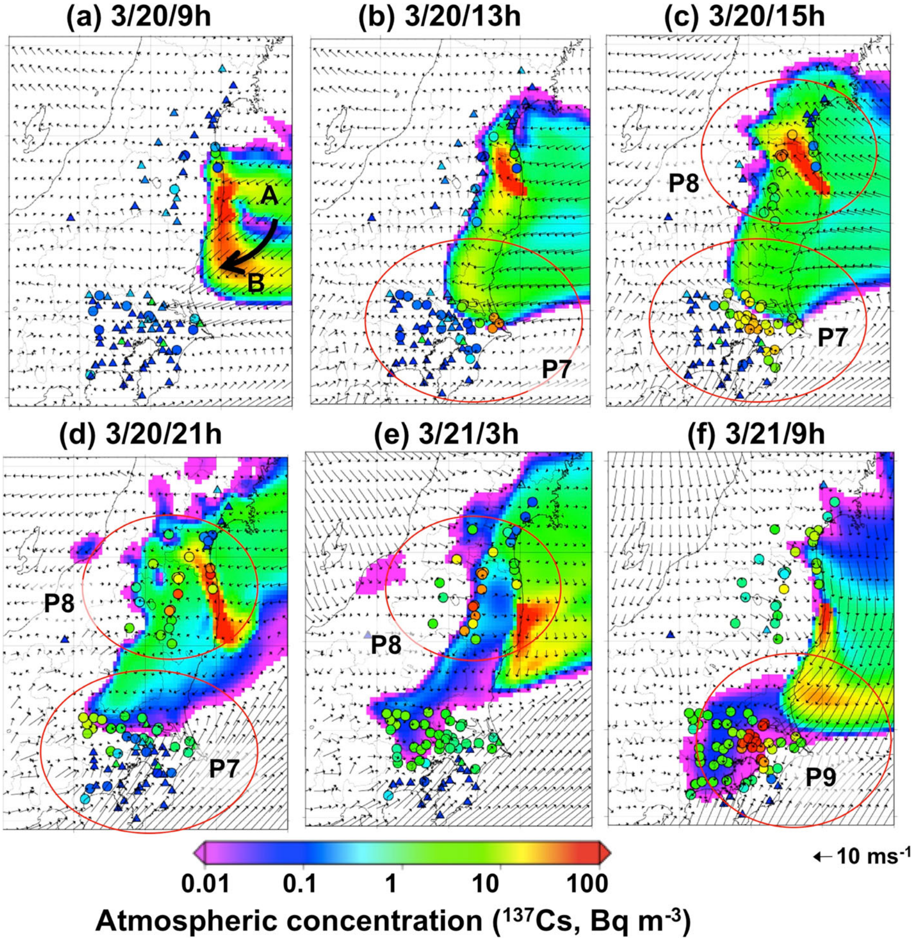

Fig. 13 a–f Maps of observations (*colored circles*) and model ensemble means of atmospheric ^{137}Cs concentration from 3/20/9 h to 3/21/9 h. Areas identified as plumes with concentration larger than 10 Bq m^{-3} are *encircled* and labeled with the name of the plume. JMA-MANAL wind vectors at 1000 hPa are superimposed. Movement of the P7 plume route is indicated by a *thick arrow* in panel **a**. See the main text for explanation of labels (**a**, **b**)

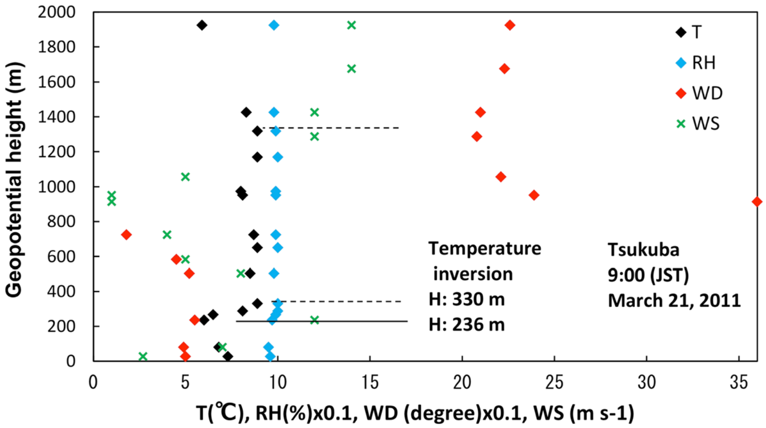

Fig. 14 Vertical profiles of temperature (*T*), relative humidity (*RH*), wind direction (*WD*), and wind speed (*WS*) versus geopotential height at 3/21/9 h for the JMA Tsukuba station. Wind directions and speeds are at the heights corresponding to the standard isobaric surfaces and characteristic points in the wind profile as determined by the JMA routine measurement protocol

explain the quick dissipation of simulated plume P7, in contrast to the observed persistent survival of the plume in the morning of 21 March (Fig. 7b, panels 3:00 to 9:00, and Fig. 13e, f).

Plume routes and time series

Figure 15 presents a summary of the plume routes analyzed in the preceding sections, and Fig. 16 shows the time series of the observations and the model ensemble mean ^{137}Cs concentrations at several sites. The relevant sites are B, C, E, and J in the Tohoku region and sites 9, 12, and 15 in the Kantou region, as defined by Tsuruta et al. (2014), as well as at the newly added sites K1, K2, and K3.

During a 6-hour period on 15 March, plume P2 spread over a large area of the Kantou region. The coverage was not uniform, and the plume was narrow, as indicated by the peak concentration at sites 9, K1, K2, and K3 in Fig. 16b. However, the simulated arrival time was too early, as indicated by the time series and as was already suggested by Fig. 9a.

Plume P3 transported the radioactive material toward the Nakadori region, crossing the Abukuma Mountains, as indicated by the successive peaks over time from the south to the north at sites E and C in the afternoon of 15 March (Fig. 16a); the models were too coarse to simulate the detailed progress of the plume along the Nakadori channel. The progress of plumes P2 and P3 is indicated by thick white arrows in Fig. 15.

As shown in Fig. 9f, plume P4 produced a high concentration of ^{137}Cs in the Choshi Peninsula, as shown by the peaks at sites 12 and 15, but the plume did not reach Kantou.

Short-duration plumes P5 and P6 were observed at site J on 18 and 19 March, and they were simulated by the models, but the simulated arrival time was earlier than the observed time. Moreover, the concentration was largely underestimated for the duration of the period.

In the early afternoon of 20 March, plume P7 was transported over a long distance, first to the ocean and then toward land by a clockwise rotation of the plume route, as indicated by the thick white arrow in Fig. 15; it covered a large part of the northern Kantou region, as shown in Fig. 16b.

Plume P8 was transported northward and was redirected southward along the Nakadori region at the northern edge of the Abukuma Mountains. Consequently, the high-concentration area moved from north to south, as illustrated by the time series of observations at sites B, C, and E. However, the models failed to indicate this phenomenon, underestimating the concentration at sites in the Nakadori region, as also shown in Fig. 7a, panels

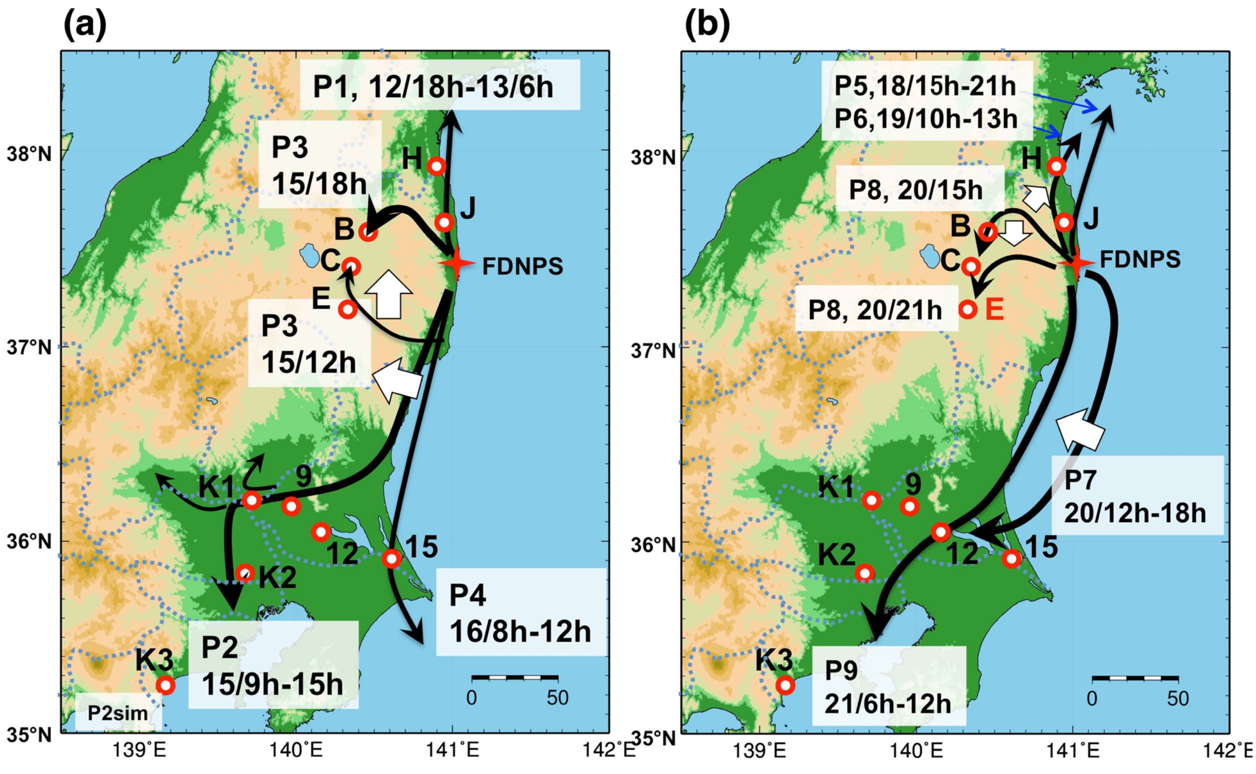

Fig. 15 a, **b** Schematic diagrams of transport routes analyzed in the present study for plumes P2, P3, P4, P7, P8, and P9. *Thick arrows* indicate the general trend of the movement of each plume

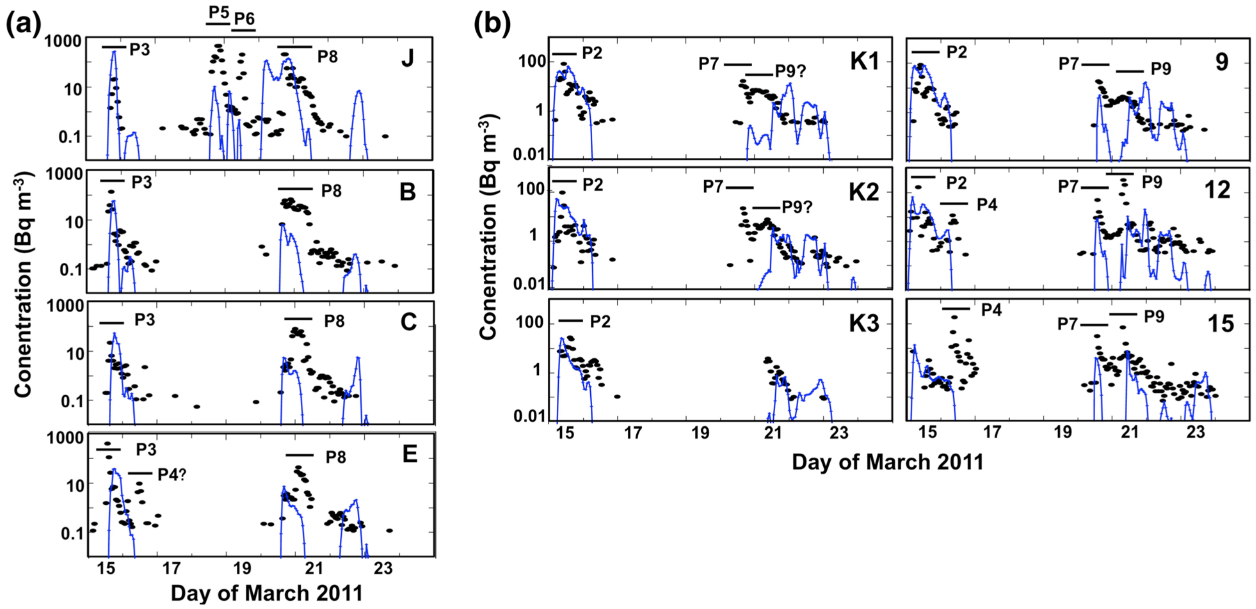

Fig. 16 Time series of observed (*dots*) and two-model ensemble mean (*lines*) atmospheric ^{137}Cs concentrations (Bq m^{-3}) from 14 to 24 March **a** in the Tohoku region at sites J, B, C, and E (see Fig. 15) and **b** in the Kantou region at sites 9, 12, 15, K1, K2, and K3 (see Fig. 15)

15:00 to 21:00. At the same time, the wind direction turned from northwest to north at the FDNPS, with the result that the northern part of P8 covered sites H and J, as illustrated by the thick northeastward arrow.

Plume P9 began on the morning of 21 March, taking a southern route until it collided with the weather front located in the southern part of the Kantou region. The simulated pattern was too short to correspond with the peaks at sites 9, 12, and 15 at 9:00; however, this is due to the complex transport and precipitation processes discussed in the preceding sections. It is difficult to determine if the peaks at sites K1 and K2 on 21 March were caused by a persistent tail from plume P7 or by plume P9, because the observed concentration remained high without a clear separation between plumes, as indicated by the distribution maps shown in Figs. 7b and 13d–f.

Conclusions

As has been discussed in the preceding sections, we found that a combined analysis of observed and model ensemble data is a useful method for analyzing the development of plumes and the distribution of radioactive materials, but neither approach alone is adequate. Although the SPM observational data are unique and of high density, they are not sufficient to show the detailed distribution structure of the atmospheric ^{137}Cs, because the transport mechanism was complex, varied over time, and depended on the local meteorological and geographical conditions. Although in some cases, the models failed to simulate the exact location and time of arrival of the plumes at the SPM sites, the spatial and temporal development of the plume structure was adequately simulated, making it possible to understand how the atmospheric ^{137}Cs was distributed.

The following statement is characteristic of the target area and period, and it is relevant to the atmospheric transportation of radioactive materials: during the analysis period in the spring season in East Asia, migratory pressure systems periodically brought radioactive materials to the Japanese land area, producing somewhat similar plume development patterns. For instance, two peaks can be seen in the time series: one due to plumes P2 and P3 followed by P4, during 15–16 March, and the other due to plumes P7 and P8 followed by P9, during 20–21 March. The first peak (P3 on 15–16 March) was caused by a change in the wind field to northeasterly and later to southeasterly, as a migratory low-pressure system progressed toward the Japanese islands. The second peaks (P4 and P9) were caused by a northerly wind after the low-pressure system had passed from the Japanese islands to the Pacific. When the height of the aerosol layer was overestimated, plumes P4 and P9 deviated eastward due to the westerly wind in the upper layers, such as at 900 hPa, as shown in Figs. 9f and 13f.

Future tasks include improving the present method, such as by conducting sensitivity tests for (1) different emission scenarios, for example, those by Katata et al. (2015); (2) plume height based on different model-layering setups; (3) wet deposition processes with different parameterizations; and (4) material transport across and along the northern edge of the Abukuma Mountains. Relevant to task 4, a report by Sekiyama et al. (2015) has claimed that there was no significant difference between 3-km and 500-m grid simulations of the JMA nonhydrostatic model for horizontal transport of radioactive material. However, in view of the differences in model parameterization for orographic waves, further analysis of this is necessary. It is also necessary to increase the spread of the model ensemble in order to obtain a more accurate reconstruction of the plume transportation. Another interesting and unresolved problem is the area of mid-level concentration, from 1 to 10 Bq m^{-3}, in the Kantou region that persisted from the evening of 20 March to the morning of 21 March. It is also important to carefully evaluate the performance of the model when simulating the vertical stratification of the atmosphere, which controls the dry deposition process. A future study should address aerosol survival under strong but stochastic precipitation conditions. On the other hand, SCJ (2014) suggested that all of the models evaluated tended to underestimate wet deposition in weak precipitation conditions. Consequently, it may be necessary to develop a nonlinear parameterization of the precipitation rate.

We have analyzed only 25% of the total SPM sampling tapes to date, so additional analysis is necessary. Further efforts are also needed to collect missing observational data, in particular, in the Hamadori region, in order to investigate the detailed atmospheric transportation processes that could not be addressed by the present study. Some of the SPM tapes were discarded by the network before we could retrieve them. Therefore, a special tape conservation effort would be required for large-scale disaster events. We expect the present study to be useful for future research.

Abbreviations

CMAQ: Community multiscale air quality; FDNPS: Fukushima Daiichi Nuclear Power Station; JAEA: Japan Atomic Energy Agency; JAXA: Japan Aerospace eXploration Agency; JMA: Japan Meteorological Agency; JST: Japan standard time; MANAL: Mesoscale objective-analysis data; MEXT: Ministry of Education, Culture, Sports, Science and Technology, Japan; NICAM: Nonhydrostatic icosahedral atmospheric model; NSW6: NICAM single-moment scheme with six water categories; SCJ: Science Council of Japan; SPM: Suspended particulate matter; SPRINTARS: Spectral radiation-transport model for aerosol species; TEPCO: Tokyo Electric Power Company; UNCEAR: United Nations Scientific Committee on the Effects of Atomic Radiation; UTC: Coordinated universal time; WRF: Weather Research and Forecast Model

Acknowledgements

We greatly appreciate the kind support of H. Tomita and H. Yashiro of RIKEN/AICS. We also thank all the local governments who offered the used SPM filter tapes at the request of the Ministry of the Environment, Japan. We have cited the weather maps of Japan Meteorological Agency. We used the meteorological data sets of the Japan Meteorological Agency.

Funding

Parts of this research were supported by funds from MOE/GOSAT2, JST/CREST/EMS/TEEDDA, JAXA/EarthCARE&GCOM-C, MEXT/KAKENHI/Innovative Areas 2409, MOEJ/ERTDF/S-12 and 5-1501, and the National Regulation Agency, Japan.

Authors' contributions

TN was the principal investigator of the modeling and SPM data analysis projects, the chair of the SCJ Model Comparison Committee, designed the combined analysis, and drafted the manuscript. SM, DG, JU, TT, and MS conducted the numerical simulations with NICAM-SPRINTARS. YM and TO conducted the numerical simulations with WRF-CMAQ. HT, TO, and ME conducted the SPM tape analysis. All co-authors participated in discussions about the results and commented on the original manuscript. All authors read and approved the final manuscript.

Authors' information

Correspondence and requests for materials should be addressed to TN (terry-nkj@nifty.com).

Competing interests

The authors declare that they have no competing interests.

Author details

[1]Atmosphere and Ocean Research Institute (AORI), The University of Tokyo, 5-1-5 Kashiwanoha, Kashiwa, Chiba 277-8568, Japan. [2]Earth Observation Research Center (EORC), Japan Aerospace Exploration Agency (JAXA), 2-1-1 Sengen, Tsukuba, Ibaraki 305-8505, Japan. [3]National Institute for Environmental Studies (NIES), 16-2 Onogawa, Tsukuba, Ibaraki 305-8506, Japan. [4]Remote Sensing Technology Center of Japan, 3-17-1 Toranomon, Minato-ku, Tokyo 105-0001, Japan. [5]Research Institute for Applied Mechanics, Kyushu University, Kasuga Park 6-1, Kasuga, Fukuoka 816-8580, Japan. [6]Graduate School of Science and Engineering, Tokyo Metropolitan University, 1-1 Minami-Osawa, Hachioji, Tokyo 192-0397, Japan.

Received: 10 June 2016 Accepted: 5 January 2017

References

Byun DW, Ching JKS (1999) Science algorithms of the EPA Models-3 Community Multi-Scale Air Quality (CMAQ) modeling system. Rep. USA EPA/600/R-99/030. US Environmental Protection Agency, Washington

Byun D, Schere KL (2006) Review of the governing equations, computational algorithms, and other components of the Models-3 Community Multiscale Air Quality (CMAQ) modeling system. Appl Mech Rev 59:51–77

Dai T, Goto D, Schutgens NAJ, Dong X, Shi G, Nakajima T (2014) Simulated aerosol key optical properties over global scale using an aerosol transport model coupled with a new type of dynamic core. Atmos Environ 82:71–82. doi:10.1016/j.atmosenv.2013.10.018

Goto D, Dai T, Satoh M, Tomita H, Uchida J, Misawa S, Inoue T, Tsuruta H, Ueda K, Ng CFS, Takami A, Sugimoto N, Shimizu A, Ohara T, Nakajima T (2015a) Application of a global nonhydrostatic model with a stretched-grid system to regional aerosol simulations around Japan. Geosci Model Dev 8:235–259. doi:10.5194/gmd-8-235-2015

Goto D, Nakajima T, Dai T, Takemura T, Kajino M, Matsui H, Takami A, Hatakeyama S, Sugimoto N, Shimizu A, Ohara T (2015b) An evaluation of simulated particulate sulfate over East Asia through global model intercomparison. J Geophys Res Atmos 120(12):6247–6270. doi:10.1002/2014JD021693

JAEA (2012) JAEA Open Workshop 'Reconstruction of the Emission and diffusion processes of materials released by the Fukushima Daiichi Atomic Power Plant accident', March 6, 2012, Tokyo, http://nsec.jaea.go.jp/ers/environment/envs/FukushimaWS/index.htm. Accessed 18 Jan 2017

Kaneyasu N, Ohashi H, Suzuki F, Okuda T, Ikemori F (2012) Sulfate aerosol as a potential transport medium of radiocesium from the Fukushima nuclear accident. Environ Sci Technol 46:5720–5726. doi:10.1021/es204667h

Katata G, Chino M, Kobayashi T, Terada H, Ota M, Nagai H, Kajino M, Draxler R, Hort MC, Malo A, Torii T, Sanada Y (2015) Detailed source term estimation of the atmospheric release for the Fukushima Daiichi Nuclear Power Station accident by coupling simulations of an atmospheric dispersion model with an improved deposition scheme and oceanic dispersion model. Atmos Chem Phys 15:1029–1070. doi:10.5194/acp-15-1029-2015

Lin YL, Farley RD, Orville HD (1983) Bulk parameterization of the snow field in a cloud model. J Clim Appl Meteorol 22:1065–1092

Mellor GL, Yamada T (1982) Development of a turbulence closure model for geophysical fluid problems. Rev Geophys Space Phys 20:851–875

Mészáros R, Leelőssy Á, Kovács T, Lagzi I (2016) Predictability of the dispersion of Fukushima-derived radionuclides and their homogenization in the atmosphere. Sci Rep 6:19915. doi:10.1038/srep19915

MEXT (2011) Airborne monitoring results after the first one conducted by the Ministry of Education, Culture, Sports, Science, and Technology in April 2011 are summarized by the Nuclear Regulation Authority. http://radioactivity.nsr.go.jp/ja/list/362/list-1.html. Accessed 6 May 2011

Morino Y, Ohara T, Nishizawa M (2011) Atmospheric behavior, deposition, and budget of radioactive materials from the Fukushima Daiichi Nuclear Power Plant in March 2011. Geophys Res Lett 38:L00G11. doi:10.1029/2011GL048689

Morino Y, Ohara T, Watanabe M, Hayashi S, Nishizawa M (2013) Episode analysis of deposition of radiocesium from the Fukushima Daiichi Nuclear Power Plant accident. Environ Sci Technol 47:2314–2322. doi:10.1021/es304620x

Nakajima T, Ohara T, Uematsu M, Onda Y (eds) (2014) Radioactive environmental pollution from the Fukushima Daiichi Nuclear Power Station accident: earth science perspectives. University of Tokyo Press, Tokyo (in Japanese)

Nakanishi M, Niino H (2004) An improved Mellor-Yamada level 3 model with condensation physics: its design and verification. Bound Layer Meteorol 112:1–31

Oura Y, Ebihara M, Tsuruta H, Nakajima T, Ohara T, Ishimoto M, Sawahata H, Katsumura Y, Nitta W (2015) A database of hourly atmospheric concentrations of radiocesium (^{134}Cs and ^{137}Cs) in suspended particulate matter collected in March 2011 at 99 air pollution monitoring stations in eastern Japan. J Nucl Radiochem Sci 15(2):1–12

Satoh M, Matsuno T, Tomita H, Miura H, Nasuno T, Iga S (2008) Nonhydrostatic Icosahedral Atmospheric Model (NICAM) for global cloud resolving simulations. J Comput Phys 227:3486–3514

SCJ (2014) A review of the model comparison of transportation and deposition of radioactive materials released to the environment as a result of the Tokyo Electric Power Company's Fukushima Daiichi Nuclear Power Plant accident, Report of Committee on Comprehensive Synthetic Engineering, Science Council of Japan, http://www.jpgu.org/scj/report/20140902scj_report_e.pdf. Accessed 18 Jan 2014

Sekiyama TT, Kunii M, Kajino M, Shimbori T (2015) Horizontal resolution dependence of atmospheric simulations of the Fukushima nuclear accident using 15-km, 3-km, and 500-m grid models. J Meteorol Soc Jpn 93:49–64

Skamarock WC, Klemp JB, Dudhia J, Gill DO, Barker DM, Duda MG, Huang XY, Wang W, Powers JG (2008) A description of the Advanced Research WRF Version 3. NCAR/TN.475 + STR. National Center for Atmospheric Research, Boulder

Sparmacher H, Fulber K, Bonka H (1993) Below-cloud scavenging of aerosol particles: particle-bound radionuclides—experimental. Atmos Environ 27(4):605–618. doi:10.1016/0960-1686(93)90218-N

Sportisse B (2007) A review of parameterizations for modelling dry deposition and scavenging of radionuclides. Atmos Environ 41:2683–2698. doi:10.1016/j.atmosenv.2006.11.057

Stohl A, Seibert P, Wotawa G, Arnold D, Burkhart JF, Eckhardt S, Tapia C, Vargas A, Yasunari TJ (2012) Xenon-133 and cesium-137 releases into the atmosphere from the Fukushima Dai-ichi nuclear power plant: determination of the source term, atmospheric dispersion, and deposition. Atmos Chem Phys 12:2313–2343. doi:10.5194/acp-12-2313-2012

Takemura T, Okamoto H, Maruyama Y, Numaguti A, Higurashi A, Nakajima T (2000) Global three-dimensional simulation of aerosol optical thickness distribution of various origins. J Geophys Res 105:17853–17873

Takemura T, Nakamura H, Takigawa M, Kondo H, Satomura T, Miyasaka T, Nakajima T (2011) A numerical simulation of global transport of atmospheric particles emitted from the Fukushima Daiichi Nuclear Power Plant. SOLA 7:101–104. doi:10.2151/sola.2011-026

Terada H, Katata G, Chino M, Nagai H (2012) Atmospheric discharge and dispersion of radionuclides during the Fukushima Dai-ichi Nuclear Power Plant accident, part II: verification of the source term and analysis of regional-scale atmospheric dispersion. J Environ Radioact 112:141–154

Tomita H, Satoh M (2004) A new dynamical framework of nonhydrostatic global model using the icosahedral grid. Fluid Dyn Res 34:357–400

Tsuruta H, Oura Y, Ebihara M, Ohara T, Nakajima T (2014) First retrieval of hourly atmospheric radionuclides just after the Fukushima accident by analyzing filter-tapes of operational air pollution monitoring stations. Sci Rep 4:6717. doi:10.1038/srep06717

Uchida J, Mori M, Suzuki K, Satoh M, Nakamura H, Nakajima T (2015) Error and energy budget analysis of a non-hydrostatic stretched-grid global circulation model. Mon Weather Rev 144:1423–1447. doi:10.1175/MWR-D-15-0271.1

Wang W, Bruyère C, Duda M, Dudhia J, Gill D, Lin H-C, Michalakes J, Rizvi S, Zhang X, Beezley JD, Coen JL, Mandel J (2012) User's guide: Advanced Research WRF (ARW) Version 3.3 modeling system. http://www.mmm.ucar.edu/wrf/users/. Accessed 12 June 2016

Yasunari TJ, Stohl A, Hayano RS, Burkhart JF, Eckhardt S, Yasunari T (2011) Cesium-137 deposition and contamination of Japanese soils due to the Fukushima nuclear accident. PNAS 108:19530–19534. doi:10.1073/pnas.1112058108

Yumimoto K, Morino Y, Ohara T, Oura Y, Ebihara M, Tsuruta H, Nakajima T (2016) Inverse modeling of the 137Cs source term of the Fukushima Dai-ichi Nuclear Power Plant accident constrained by a deposition map monitored by aircraft. J Environ Radioact 164:1–12